Electronic Supplementary Information(ESI)

Heterolayered 2D nanohybrids of uniformly-stacked transition metal dichalcogenide–transition metal oxide monolayers with improved energy-related functionalities

Xiaoyan Jin,[a] Seung-Jae Shin,[b] Jungeun Kim,[a] Nam-Suk Lee,[c] Hyungjun Kim,[b] and Seong-Ju Hwang[a,*]

[a] Center for Hybrid Interfacial Chemical Structure (CICS), Department of Chemistry and Nanoscience, College of Natural Sciences, Ewha Womans University, Seoul 03760, Republic of Korea

[b] Department of Chemistry, Korea Advanced Institute of Science and Technology (KAIST), Daejeon 34141, Republic of Korea

[c] National Institute for Nanomaterials Technology (NINT), Pohang University of Science and Technology (POSTECH), Pohang 37673, Republic of Korea

Table S1. Zeta potential data of the colloidal suspensions of exfoliated MoS_2 and MnO_2 nanosheets (NSs), and their mixtures.

Material	MoS_2 NS	MnO_2 NS	MnO_2/MoS_2 (0.5/100)	MnO_2/MoS_2 (1/100)	MnO_2/MoS_2 (2/100)
Zeta potential (mV)	–41	–50	–41	–41	–41

: The surface charges of exfoliated MoS_2 and MnO_2 NSs are examined with zeta potential measurements. As listed in Table S1, the colloidal suspensions of exfoliated MoS_2 and MnO_2 NSs, and their colloidal mixtures show distinct negative zeta potentials, indicating the negative surface charges of these NSs.

Fig. S1. (a) Contact angles of exfoliated MoS_2 and MnO_2 NSs, and their mixture (MoS_2/MnO_2). (b) Transmission electron microscopy (TEM) images, and (c) size distribution curves of exfoliated MoS_2 and MnO_2 NSs.

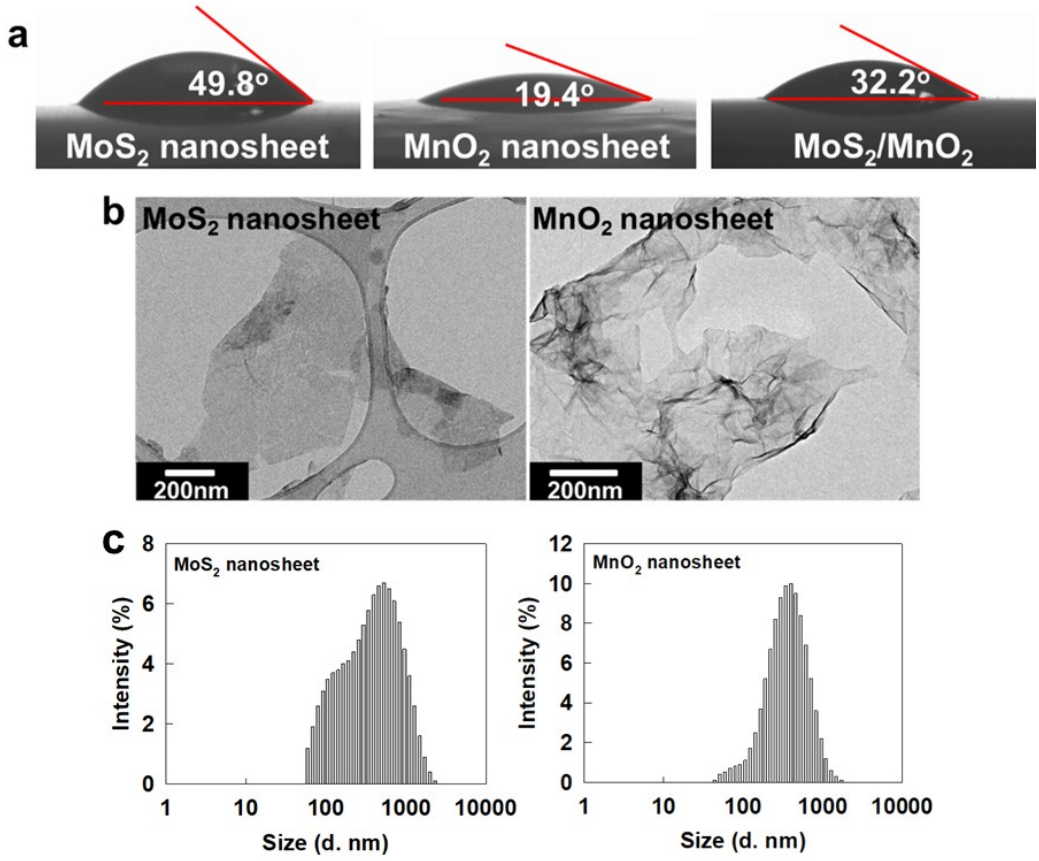

: The surface hydrophilicities and crystal dimensions of MoS_2 and MnO_2 NSs are probed with contact angle measurements and TEM analysis. As illustrated in Fig. S1a, both the exfoliated MoS_2 and MnO_2 NSs show small contact angles of ~20–50°, indicating the hydrophilic surface natures of both NSs. The TEM images of Fig. S1b clearly demonstrate the highly anisotropic 2D morphologies of the exfoliated MoS_2 and MnO_2 NSs. As can be seen from the size distribution curves of Fig. S1c, both the exfoliated MoS_2 and MnO_2 NSs possess similar lateral dimensions of several hundreds of nanometers.

Fig. S2. (a) Mo K-edge and (b) Mn K-edge X-ray absorption near-edge structure (XANES) spectra of the **HMM** nanohybrids and several references.

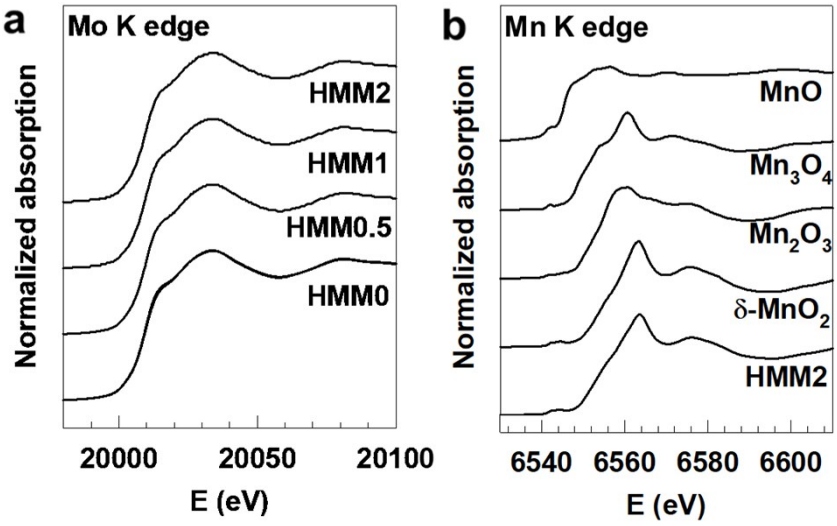

: The electronic and local crystal structures of MoS_2 and MnO_2 components in the present **HMM** nanohybrids are examined with Mo K-edge and Mn K-edge XANES spectroscopies, respectively. As illustrated in Fig. S2a, all the **HMM** nanohybrids display typical Mo K-edge XANES spectral features to those of MoS_2 phase, confirming the maintenance of the original MoS_2 structure upon the hybridization with MnO_2 NS. Similarly, the Mn K-edge XANES spectrum of **HMM2** nanohybrid is nearly identical to that of the reference layered δ-MnO_2 phase, see Fig. S2b. This result clearly demonstrates the retention of the layered structure of MnO_2 NS after the hybridization with MoS_2 NS.

Fig. S3. Mn 3s X-ray photoelecton spectra (XPS) data of H-MnO_2 and **HMM1** nanohybrid.

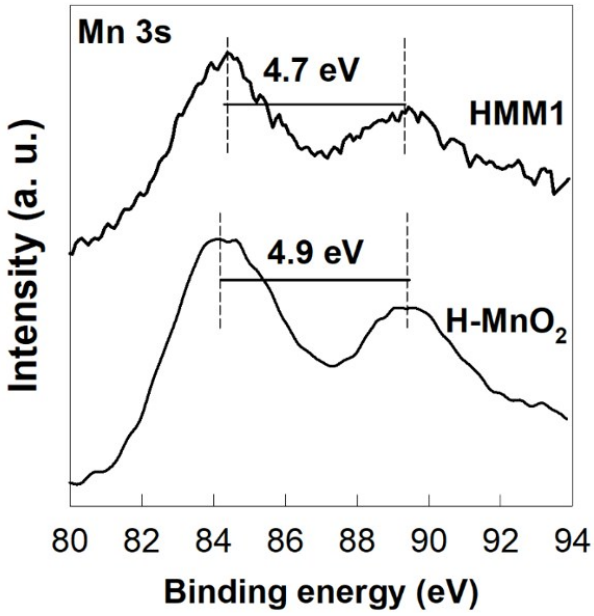

: The electron transfer between restacked MnO_2 and MoS_2 nanosheets is quantified with the Mn 3s XPS results. As shown in Fig. S3, the peak spin-energy separation (ΔE) is determined as 4.9 eV for of H–MnO_2 having the average Mn oxidation state of ~3.8.[1,2] In the case of **HMM1** nanohybrid, ΔE is estimated as 4.7 eV, indicating the average Mn oxidation state of ~4.0.[3] This result clearly demonstrates the occurrence of ~0.2 electron transfer into each MnO_2 nanosheet in the **HMM1** nanohybrid.

Fig. S4. Mo 3d XPS of **HMM** nanohybrids.

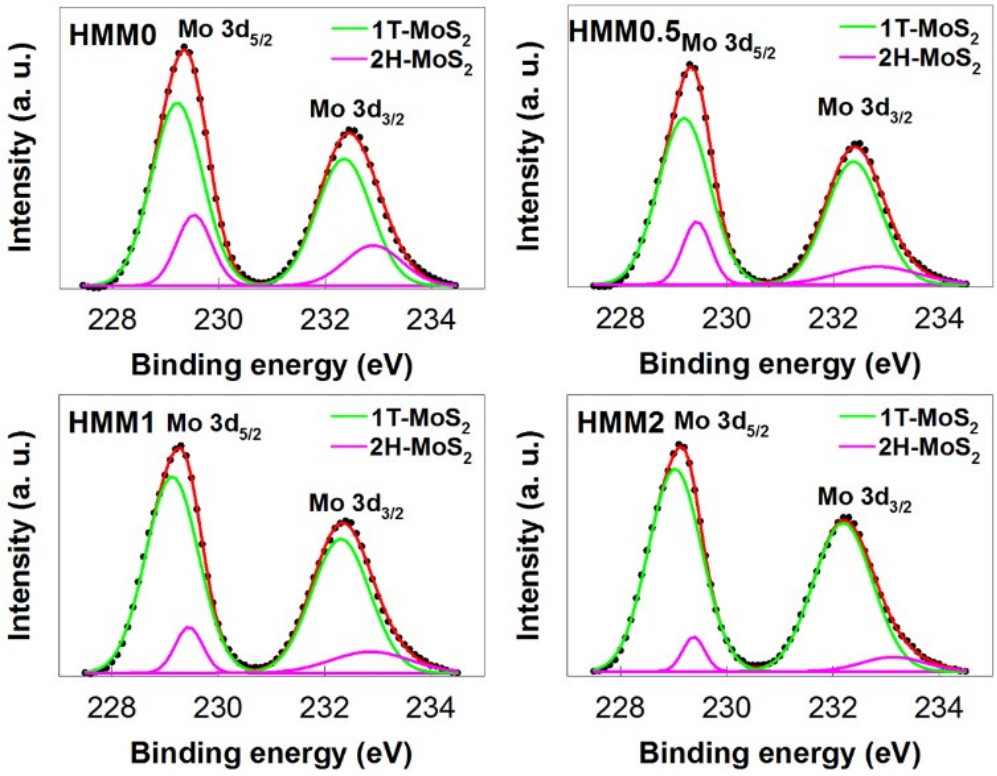

Table S2. Relative concentrations of 1T and 2H MoS_2 in the present **HMM** materials determined by Mo 3d XPS results.

	HMM0	**HMM0.5**	**HMM1**	**HMM2**
1T MoS_2	77.3%	79.6%	86.1%	90.4%
2H MoS_2	22.7%	20.4%	13.9%	9.6%
Total	100%	100%	100%	100%

: The relative ratios of 1T- and 2H-MoS_2 phases in the present **HMM** nanohybrids are estimated by peak convolution analysis for Mo 3d XPS data. As presented in Fig. S4 and Table S2, the peak deconvolution analysis of Mo 3d XPS data indicates the co-existence of metallic 1T phase and semiconducting 2H MoS_2 in the **HMM** nanohybrids and the increase of 1T MoS_2 amount upto >90% upon the hybridization with MnO_2 NS. This result underscores the stabilization of the 1T structure of exfoliated MoS_2 NS by the intervened MnO_2 NS due to the depressed stacking of MoS_2.

Fig. S5. Atomic model of MoS_2–MnO_2 interface employed in density functional theory (DFT) calculations. (a) Intercalated protons are conceived to interact with the MnO_2. DFT-optimized interface models of (b) 1T MoS_2–MnO_2 and (b) 2H MoS_2–MnO_2. We first optimized MnO_2 and MoS_2, yielding lattice parameters of 2.91 Å for MnO_2, 3.24 Å for 1T MoS_2, and 3.18 Å for 2H MoS_2. Then, two layers of MnO_2 and MoS_2 are assembled in the orthorombic super cell, which consists of two formula units of MnO_2 and MoS_2. To reconcile the lattice mismatch between MnO_2 and MoS_2, MnO_2 structures are under ~10% of tensile strain in order to have the same lattice parameters as MoS_2 considering the much larger MoS_2 contents in nanohybrids. Also, the metal centers of Mn and Mo are located in the staggered orientations. DFT-calculated charge difference before and after two heterolayers are assembled for (c) 1T MoS_2–MnO_2 hybrid system, (d) 2H MoS_2–MnO_2 hybrid system, and (e) their comparison using in-plane averaged value. More profound charge transfer from MnO_2 to MoS_2 is found for 1T MoS_2 case.

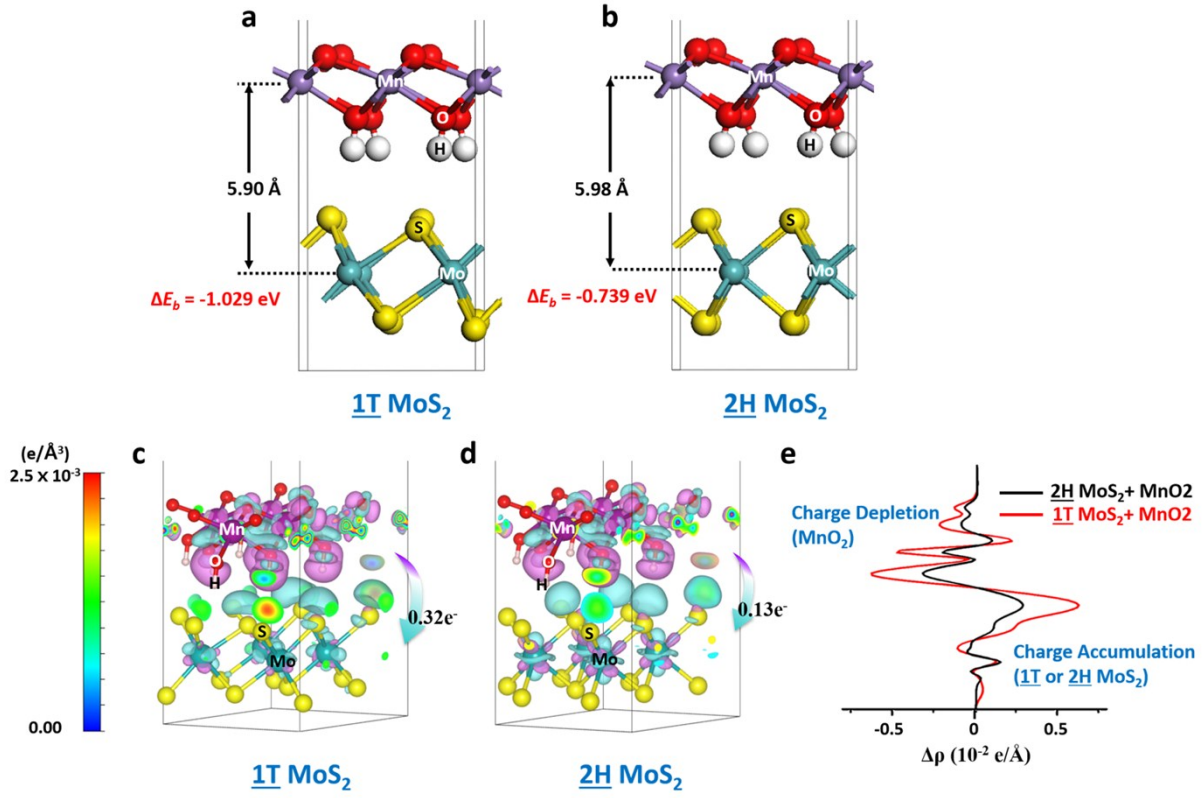

Fig. S6. k^3-weighted Mo K-edge extended X-ray absorption fine structure (EXAFS) oscillations of the **HMM** nanohybrids.

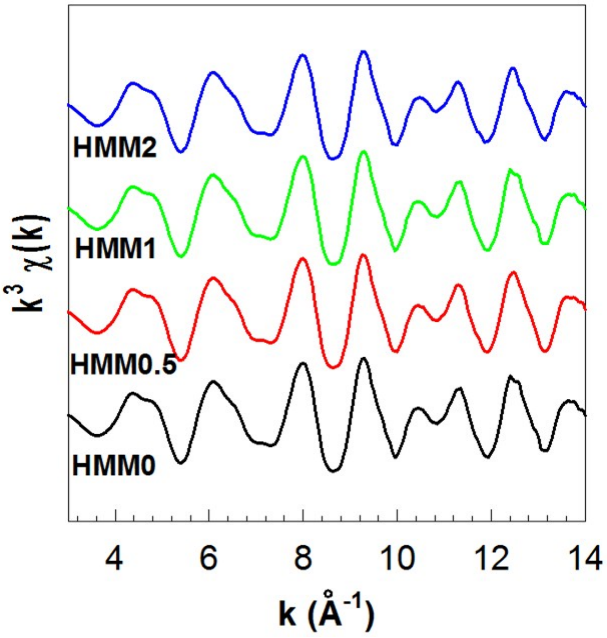

: The local atomic arrangement around Mo ion in the present **HMM** nanohybrids is investigated with Mo K-edge EXAFS analysis. As plotted in Fig. S6, regardless of the amount of MnO_2 NS, all the **HMM** nanohybrids exhibit almost the same Mo K-edge EXAFS oscillations typical of MoS_2 phase, indicating the negligible effect of hybridization with MnO_2 NS on the local crystal structure of MoS_2 NS.

Fig. S7. (a) Atomic force microscopy (AFM) images and (b) height profiles of the **HMM0** and **HMM1** nanohybrids.

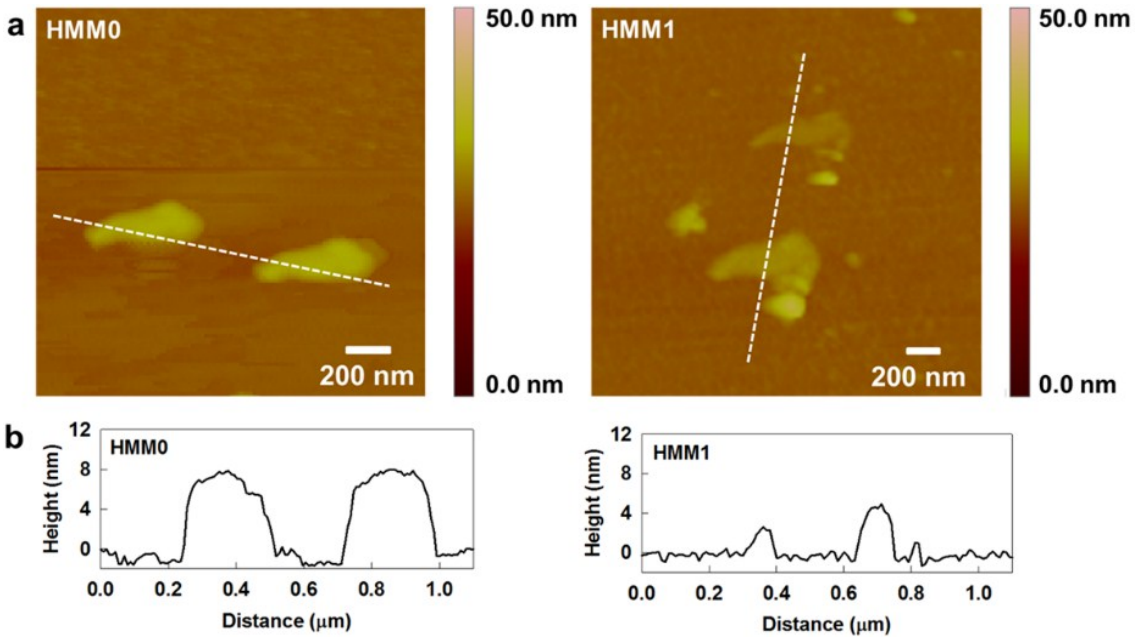

: The crystal shape and layer thickness of the **HMM0** and **HMM1** nanohybrids are probed by AFM analysis. As illustrated in Fig. S7, both materials commonly show highly anisotropic 2D crystal morphologies with thin thickness of several nm. The MnO_2 NS-incorporated **HMM1** nanohybrid shows notably thinner thickness than does the MnO_2 NS-free **HMM0** nanohybrid, indicating the decrease of the stacking number of MoS_2 NS upon hybridization with MnO_2 NS.

Fig. S8. N_2 adsorption–desorption isotherms of the **HMM** nanohybrids.

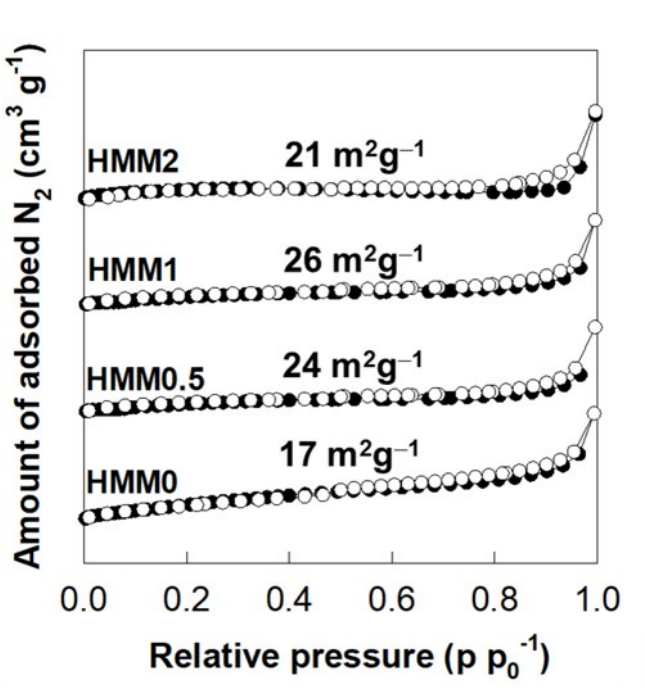

: The surface areas of the present **HMM** nanohybrids are studied with N_2 adsorption–desorption isotherm measurements. As plotted in Fig. S8, all the present nanohybrids commonly show distinct N_2 adsorption. According to the surface area calculation based on Brunauer–Emmett–Teller (BET) equation, the incorporation of MnO_2 NS leads to the notable increase of surface area of restacked MoS_2 NSs.

Fig. S9. Field emission-scanning electron microscopy (FE-SEM) images of the **HMM** nanohybrids and the precursor MoS_2 and MnO_2 NSs.

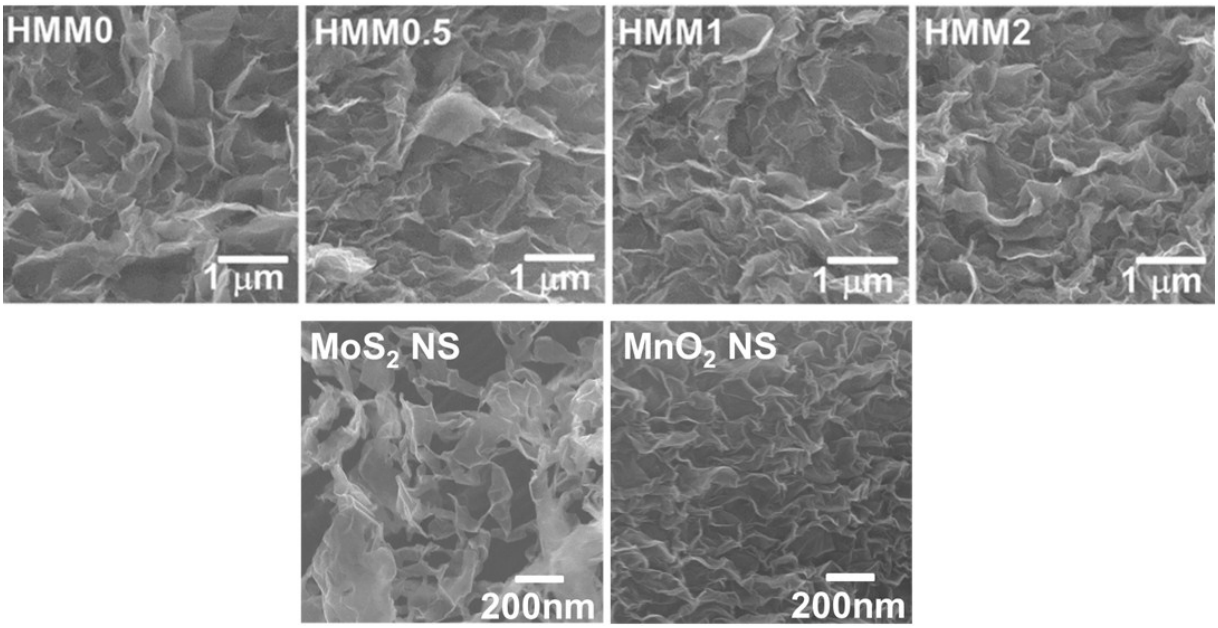

: The crystal morphologies of the present **HMM** nanohybrids as well as the precursors MoS_2 and MnO_2 NSs are probed with FE-SEM analysis. As depicted in Fig. S9, all the present materials commonly show porous morphology composed of house-of-cards-type stacking structure of NSs.

Fig. S10. Powder X-ray diffraction (XRD) patterns of (a) **HMM0** and (b) **HMM1** nanohybrids in 0.5 M H_2SO_4 electrolyte before and after hydrogen evolution reaction (HER) test.

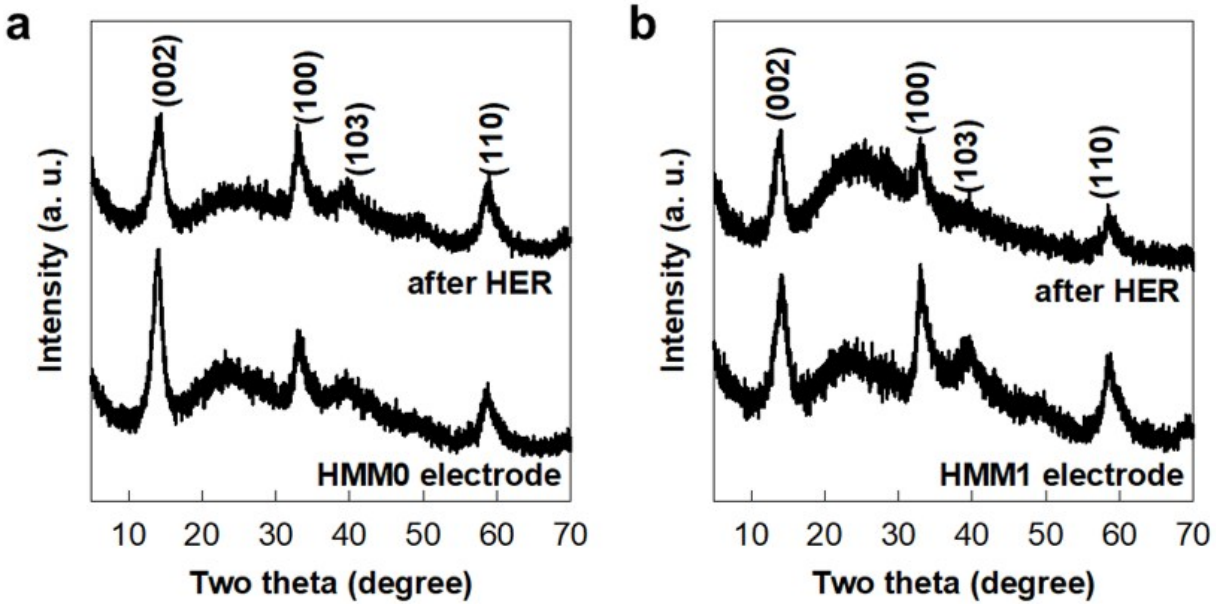

: Fig. S10 displays the powder XRD patterns of **HMM0** and **HMM1** electrocatalysts before and after the HER process. The high electrochemical stabilities of **HMM** nanohybrids are clearly evidenced by no notable change in their XRD patterns before and after the HER process. This indicates the maintenance of the crystal structures of the **HMM** nanohybrids during the HER process. In all the present XRD patterns, the broad feature originating from the glass holder is discernible at 2θ = ~20–30° due to the incomplete coverage of glass holder caused by small amount of electrocatalyst materials.

Table S3. Results of non-linear least-squares curve fittings for *in-situ* Mo K-edge EXAFS spectra of the **HMM0** and **HMM1** nanohybrids measured at several potentials of 0, –0.25, and –0.45 V during the HER process.

Material	Bond	R (Å)	σ^2 ($10^{-3} \times$ Å^2)
HMM0 0 V [a]	(Mo–S)	2.404	3.06
	(Mo–Mo)	3.164	5.60
HMM0 –0.25 V [b]	(Mo–S)	2.407	3.12
	(Mo–Mo)	3.164	5.63
HMM0 –0.45 V [c]	(Mo–S)	2.403	3.02
	(Mo–Mo)	3.162	5.53
HMM1 0 V [d]	(Mo–S)	2.407	3.56
	(Mo–Mo)	3.151	7.26
HMM1 –0.25 V [e]	(Mo–S)	2.406	3.76
	(Mo–Mo)	3.149	7.51
HMM1 –0.45 V [f]	(Mo–S)	2.406	3.63
	(Mo–Mo)	3.151	7.48

The curve fitting analysis was performed for the range of [a] 1.104–R–3.651 Å and 2.900–*k*–12.700 Å^{-1}; [b] 1.074–R–3.620 Å and 2.900–*k*–12.700 Å^{-1}; [c] 1.043–R–3.620 Å and 2.900–*k*–12.700 Å^{-1}; [d] 1.043–R–3.743 Å and 2.950–*k*–12.700 Å^{-1}; [e] 1.074–R–3.743 Å and 2.900–*k*–12.700 Å^{-1}; [f] 1.043–R–3.651 Å and 2.900–*k*–12.700 Å^{-1}.

Table S4. Zeta potential data of the colloidal suspensions of various exfoliated transition metal dichalcogenide (TMD) and transition metal oxide (TMO) NSs, and their mixtures.

Material	MoS_2 NS	MnO_2 NS	RuO_2 NS	TiO_2 NS	WS_2 NS
Zeta potential (mV)	–41	–50	–50	–44	–38
Material	MoS_2/TiO_2 NS	MoS_2/RuO_2 NS	WS_2/MnO_2 NS	WS_2/TiO_2 NS	WS_2/RuO_2 NS
Zeta potential (mV)	–42	–41	–38	–39	–39

: The surface charges of various exfoliated TMD and TMO NSs are examined with zeta potential measurements. As listed in Table S4, the colloidal suspensions of exfoliated MoS_2/WS_2 and $TiO_2/MnO_2/RuO_2$ NSs, and their colloidal mixtures show distinct negative zeta potentials, indicating the negative surface charges of these NSs.

Fig. S11. Contact angles of various TMD NSs and mixed TMD–TMO NSs.

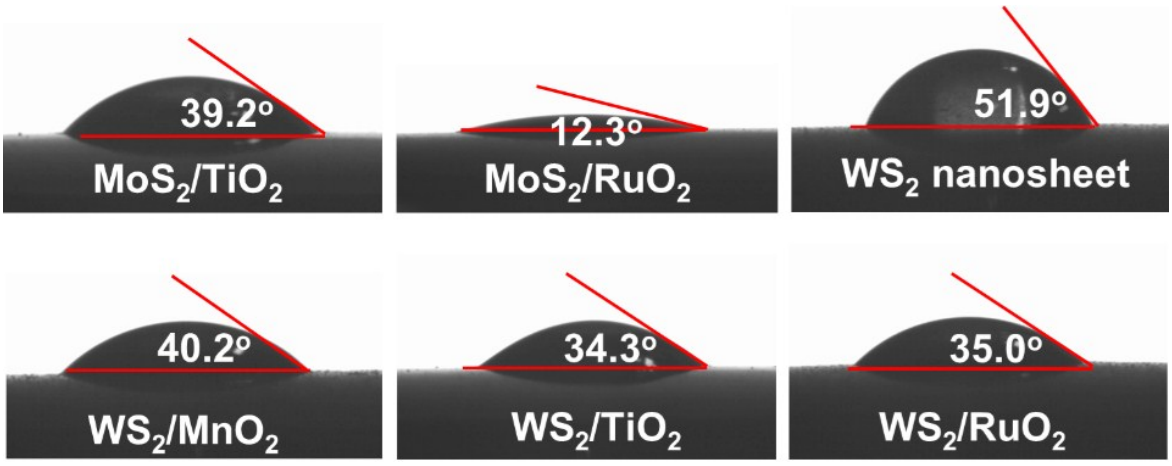

: The surface hydrophilicities of various TMD NSs and mixed TMD–TMO NSs are probed with contact angle measurement. All the present colloidal mixtures of TMD–TMO NSs possess negative surface charge and significant hydrophilicity.

Fig. S12. (a) Powder XRD patterns, (b) FE-SEM image, and (c) cyclic voltammetry (CV) curves of the H–MoS_2 and H–MoS_2–RuO_2 nanohybrids.

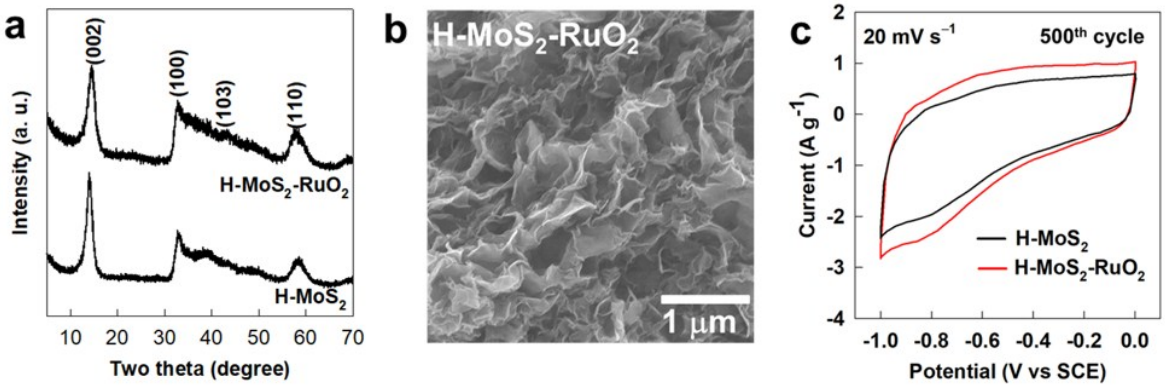

: As shown in Fig. S12, the restacked H–MoS_2 and H–MoS_2–RuO_2 nanohybrids synthesized from these colloidal mixtures show the c-axis-vertically-ordered heterostructures of TMD and TMO NSs with porous stacking morphologies. The incorporation of RuO_2 NS into the restacked MoS_2 NSs leads to the decrease of basal spacing, reflecting the replacement of thicker MoS_2 layer with thinner RuO_2 layer. The restacked H–MoS_2–RuO_2 nanohybrid delivers a larger specific capacitance than does H–MoS_2 NS, indicating the improvement of supercapacitor electrode functionality of MoS_2 upon the hybridization with RuO_2 NS.

References

1 B. Xu, L. Yu, M. Sun, F. Ye, Y. Zhong, G. Cheng, H. Wang, Y. Mai, *RSC Adv.* 2017, **7**, 14910.

2 M. Toupin, T. Brousse, D. Bélanger, *Chem. Mater.* 2004, **16**, 3184.

3 Z. Lei, J. Zhang, X. S. Zhao, *J. Mater. Chem.* 2012, **22**, 153.